# NEW FEMTOSECOND PULSE SEQUENCE PROCESSING POSSIBILITIES USING A DOUBLE PASSED ARRAYED WAVEGUIDE GRATING: ENGINEERING APPROACH BASED ON OPTIMIZATION

A Thesis

Submitted to the Faculty

of

Purdue University

by

Bhaskaran Muralidharan

In Partial Fulfillment of the

Requirements for the Degree

of

Master of Science in Electrical and Computer Engineering

August 2003

*To my grand parents*

## ACKNOWLEDGMENTS

This work has been accomplished with assistance and inspiration from several sources. First and foremost, I would like to thank Professor Andrew Weiner, for his idea and regular meetings which made this work possible. I would like to extend my very special regards to Professor Venkataramanan Balakrishnan for his constant help during a considerable part of this work. It had been an invaluable experience to feel the excitement of working in two different areas of interest. I would like to thank my other committee member Prof. Shalaev who agreed to participate in the final overview of this project. It has also been highly stimulating to interact with my group members through various group meetings, and discussions. Of course, I thank Purdue community due to which I have made some invaluable friends. lastly, I would like to acknowledge the life, works, and achievements of inspiring people, that I am constantly made aware of, which in turn inspires me to try and realize my goals.

TABLE OF CONTENTS

Page

# LIST OF TABLES

# LIST OF FIGURES

# ABSTRACT

Muralidharan, Bhaskaran. M.S.E.C.E, Purdue University, August, 2003. New Femtosecond Pulse Sequence Processing Possibilities Using a Double Passed Arrayed Waveguide Grating: Engineering approach based on Optimization . Major Professor: Andrew. M. Weiner.

Very recently, the Arrayed Waveguide Grating (AWG) has been experimented for its ability to generate high repetition rate Wavelength Division Multiplexed (WDM) pulse trains. Double passing the AWG results in very high repetition rate pulse bursts on multiple wavelength channels that combine together to generate multi wavelength waveforms over very large time windows. Many applications, especially in Wavelength Division Multiplexing, demand waveforms that are flat topped. However, only limited effort has been made to engineer the AWG device, in order to generate such flat topped pulse trains. Our work, develops innovative designs such that the AWG generates almost flat topped pulses on double pass, based on the technique of numerical optimization. Efficient low loss designs, robust to limits of fabrication errors are presented, along with detailed selection criteria for possible designs. Also, these designs are based on the 'Phase only' approach, which is convenient from the fabrication point of view, thus opening strong possibilities for experimental verification, and eventual deployment.

# 1. INTRODUCTION

The ability to generate femtosecond pulses has been extremely useful in different domains of research. The applications range from communications to spectroscopy. Short pulses with high repetition rate determine the capacity of optical communications. Bursts of short pulses are used for spectroscopic analysis. Many such widespread applications can be thought of. This thesis explores the possibilty of generation of a multi wavelength ultra high bit rate pulse train that is also wide spread in time domain. This thesis is a simulation based investigation of the aforementioned functionality using a double passed Arrayed Waveguide grating. The approach used here is the technique of numerical optimization. The designs generated show strong prospects for experimental verification and eventual deployment.

## 1.1 The Problem Narrated

The Arrayed Waveguide grating (AWG) is a Wavelength Division Multiplexing (WDM) device. Traditionally it is used to separate one wavelength from another. In its usual configuration, the device accepts a source of light (which consists of multiple wavelengths) as its input, and each of the N outputs consists of the separated wavelength. A schematic of the device is shown in fig. 1.1 A completely new functionality of the device had been experimentally realized in 2001 [1-3], in which the device was tested for a time domain functionality. The AWG was used to generate a burst of pulses starting off from a single pulse. In other words if we come up with one pulse as the input the output would be a short burst of a few tens of pulses. Each of the $N$ outputs of the AWG generates one such identical pulse burst, although shifted in wavelength. Hence if we recombine these bursts using a double pass system (as illustrated in Fig.1.2), we can recombine the pulse bursts with suitable delay. This would

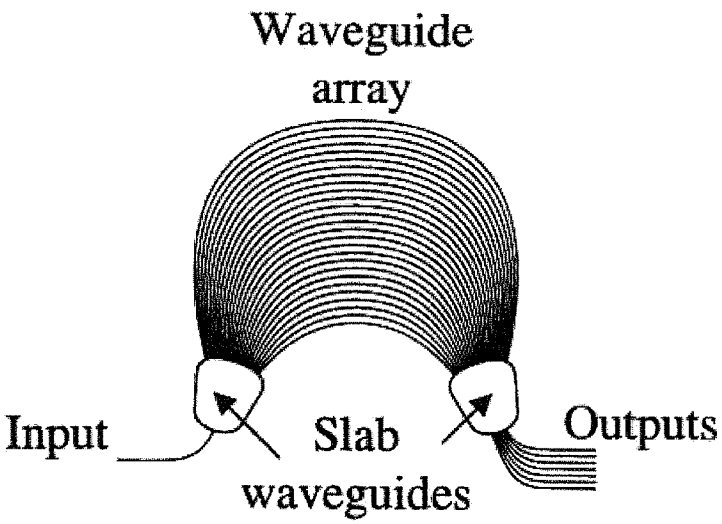


Fig. 1.1. Layout of the AWG device. Ref. Leaird et.al. [2]

result in a long pulse train that has resulted from a single pulse at the input. This experiment thus opens completely new possibilities for femtosecond pulse processing using integrated optics. Several bulk optics based pulse processing technologies have been explored [4-6]. However, only limited work has been reported on integrated optic implementation of pulse shapers typically using AWGs.

It can be understood with a little observation that the output of a double pass system can be modeled as a double auto convolution of the impulse response of the device (under suitable assumptions as discussed in a future chapter). We know from the thoery of convolutions that a square waveform when convolved with itself will generate a triangular waveform. It has been verified [3] that a single pulse input to the device generates a square pulse train in the single pass and consequently a series of wavelength shifted triangular bursts on double pass. However we realize that most pulse processing applications (especially in communications) require that we have a large burst of flat topped pulses. The advantages of double passed system is two fold: firstly as was stated earlier, that of generating a large multiwavelength burst of pulses

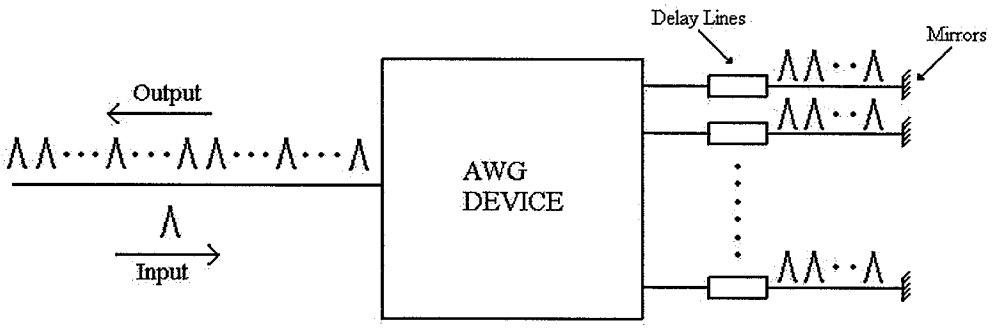


Fig. 1.2. Block Diagram of a Double passed configuration using AWGs.

starting off with a single pulse. Secondly, The possibility of engineering a phase only system using standard AWGs. (more of this will be covered in the theory section). In other words the aim of this thesis is to design a double passed AWG system that realizes an almost 'flat topped burst of pulses on double pass. Fig. 1.2, shows the block diagram of this problem. The double pass configuration is realized by reflecting each of the single pass ouputs back into the device, with sufficient delays. Hence the output will be a long train of pulses, each part being reflected off from a particular output waveguide. This figure is a pictorial narrative of the problem.

The technique used in our design is of numerical optimization. The results obtained seem satisfactory to a level of design and takes into account fabrication too.

## 1.2 Layout of the thesis

The next few chapters discuss the extent of the thesis in great detail. The second chapter deals with the theory of AWGs and a brief description of some of the first few experiments in the area of pulsed AWG. Chapter 3 delves into the mathematical aspects that are involved in the optimization approach. Here, we also discuss in brief the optimization approach as applied to the present problem. chapter 4 has been

devoted to the discussion and interpretation of the simulation results. Finally, future directions of our work is discussed.

# 2. THE ARRAYED WAVEGUIDE GRATING

This chapter is devoted to the understanding of the working principles of the Arrayed Waveguide Grating (AWG). Most of this chapter deals with basic working principles of the device used traditionally as a wavelength de-multiplexer. At the end of the chapter, we shall discuss recent experiments that explore the time domain functionality of the AWG. After that, we will be in a position to understand the systems based design approach that is covered in the next chapter.

## 2.1 The AWG explained

The AWG is an integrated optic device[13], [14]. It is also known as Phased Arrays (PHASARs). AWGs concept was first proposed in 1988 by Smit [7]. Fig. 2.1 shows the layout of an AWG. It consists of input/output waveguides, two focusing planar slab regions, and a phase array of multiple channel waveguides. In the normal configuration the device consists of one input and several outputs (a $1 \times N$ configuration). The operation is understood as follows. When the beam propagating through the transmitter waveguide enters the Free Propagation Region (FPR, the input slab and the output slab), it is no longer laterally confined and becomes divergent. On arriving at the input aperture the beam is coupled into the waveguide array and propagates through the individual waveguides to the output aperture. The length of the array waveguides is chosen such that the optical path length difference $\Delta L$ between adjacent waveguides equals an integer multiple $m$ of the central wavelength of the demultiplexer. For this wavelength, the fields in the individual waveguides will arrive at the output aperture with equal phase (apart from an integer multiple of $2\pi$), and the field distribution at the input aperture will be reproduced at the output aperture. The divergent beam at the input aperture is thus transfromed into a convergent one

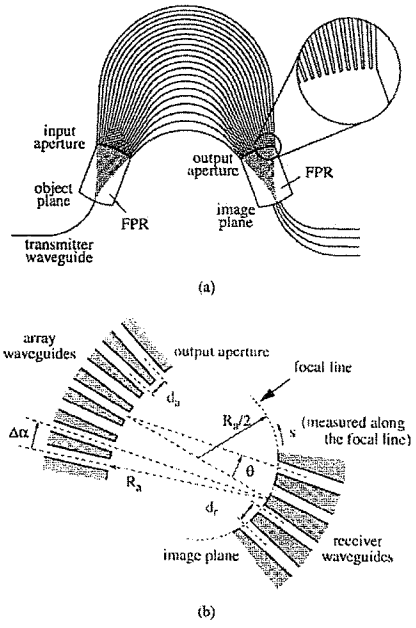


Fig. 2.1. a) Layout of the AWG. b) Geometry of the reciever side. Ref. Smit et.al. [8]

with equal amplitude and phase distribution, and an image of the input field at the object plane will be formed at the center of the image plane. The two important properties of the AWG will be analyzed in the following subsections:

### 2.1.1 A. Focusing

Focusing is obtained by choosing the length difference $\Delta L$ between adjacent array waveguides equal to an integer number of wavelengths, measured inside the array waveguides:

$$\Delta L = m\frac{\lambda_c}{N_g} \tag{2.1}$$

in which $m$ is the order of the phased array, $\lambda_c$ is the central wavelength in vacuum, and $N_g$ is the effective index of the waveguide mode. With this choice the array acts as a lens with image and object planes at a distance $R_a$ of the array apertures. The focal line of the input or output aperture defines the image plane, thus transmitter or reciever waveguides should be positioned along that line. If the wavelength is changed the focal field of the AWG moves along the receiver waveguides. This can be expressed as a dispersion relation [13] for $\theta$ (fig. 2.1 (b)):

$$\frac{\beta\Delta L}{\beta_{FPR}} - d_a sin(\theta) = \frac{m2\pi}{\beta_{FPR}} \tag{2.2}$$

in which, $\beta$ and $\beta_{FPR}$ are the propagation constants of the waveguide mode and the slab mode in the free propagation region (FPR), respectively, and $d_a$ is the lateral spacing of the waveguides in the array aperture. This equation shows that for each value of $\theta$ there is a wavelength satisfying the phase match condition. Thus each receiver waveguide at the output section receives a unique frequency. Thus the AWG functions as a wavelength demultiplexer.

### 2.1.2 B. Free Spectral Range

From Fig. 2.1(b) and Eqn. 2.5, it is seen that the angle $\theta$ decides the position of the output waveguide with respect to frequency. Also the phase difference $\Delta\Phi$

between adjacent waveguides is related to the delay length increment $\Delta L$ between them by:

$$\Delta\Phi = \beta\Delta L \tag{2.3}$$

here $\beta$ is the propagation constant of the waveguide mode. The condition for constructive interference at the output waveguides is satisfied for multiple orders $m$ (based on diffraction theory), determined by the fact that for each change of $2\pi$ in $\Delta\Phi$ the field will be imaged at the same position. This period in the frequency domain, (in other words the shift in frequency after which the field will be imaged at the same position $\theta$) is called as the Free Spectral Range or FSR, given by:

$$\Delta f_{FSR} = \frac{c}{N_g \Delta L} \tag{2.4}$$

This FSR is also related to the time delay increment between two adjacent waveguides:

$$\Delta f_{FSR} = \frac{1}{\Delta\tau} \tag{2.5}$$

where $\Delta\tau$ is the time delay increment between adjacent waveguides in the array. We will see that this parameter shall play a crucial role in our application of AWGs for time domain pulse shaping.

## 2.2 Pulsed AWG: Experiments

In the last section we saw that the AWG is used as a wavelength de-multiplexer based on the fact that different frequencies are received based on the angle $\theta$ at which the output waveguides are placed. This is a frequency domain application, and thus one of the main application of the AWG that has been put to commercial use [13-15]. However we also note that the waveguides in the array are optical 'delay lines', in a sense that a sufficiently small pulse shall get delayed by different amounts (given by the delay increment $\Delta\tau$ for each pair of adjacent waveguides). In other words, a single pulse at the input splits into several pulses due to the fact that each part of the beam undergoes different delays at different waveguides in the array. Hence

each of the output waveguides recieves a wavelength shifted copy of a similar burst of pulses. However it should be noted that the excitation profile of the beam is usually Gaussian, hence the output pulse sequence has a Gaussian envelope. Of course the temporal envelope is calculated from a measurement of a single passband in the power spectrum. This time domain application was experimentaly verified [1] recently. For short pulse applications, the important AWG parameter determining the character of the output is the free spectral range (FSR), which is equal to the inverse of the delay increment per guide ($\Delta\tau$) (as noted in the previous section). In traditional AWG devices, the FSR is typically required to be large to ensure that a unique output wavelength is present at each output, of course each wavelength complying to the requirements of the WDM system. For the generation of such trains of femtosecond pulses, we work in the opposite regime, where the optical bandwidth, $\Delta\nu$ exceeds the FSR. In other words the pulse width of the input pulse is less than the delay increment per guide. This seems to be a reasonable assumption as each pulse must travel completely through the delay line so that distinct pulses appear as shifted versions of the same pulse, after traversing through the waveguides in the array.

In summary, the experiments [1], have shown that generation of trains of femtosecond pulses at Terahertz repetition rates is possible from an AWG. The key requirements are that the FSR of the device must be tailored such that the pulse width of each pulse is much smaller than the delay increment per waveguide. This delay increment will be the temporal spacing between adjacent pulses of the train. The output temporal profile depends on the excitation profile at the input of the waveguide array (which is most naturally of the Gaussian form). The output temporal profile is invariant across different outputs of the same device, but the central wavelength shifts from one output to the next with the amount of shift given by the channel spacing of the device. The pulse width of the individual pulse is given determined by the input pulse width. Fig. 2.2 displays the expected output profile in time and frequency domain. Fig. 2.3 shows a few experimental traces.

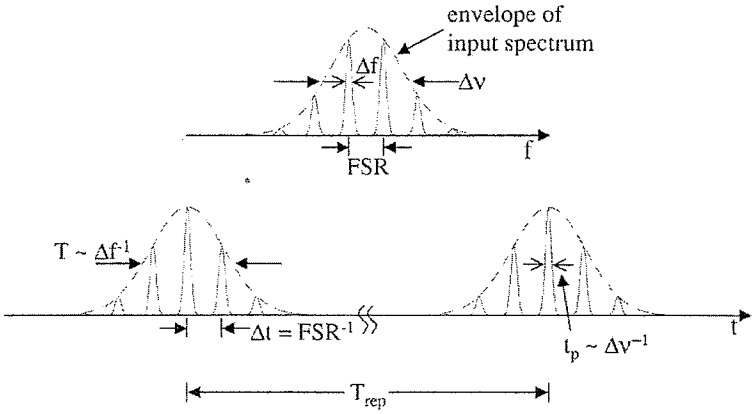


Fig. 2.2. Expected output spectrum and temporal profile for an arbitrary output guide of the AWG. Ref. Leaird et.al [1]

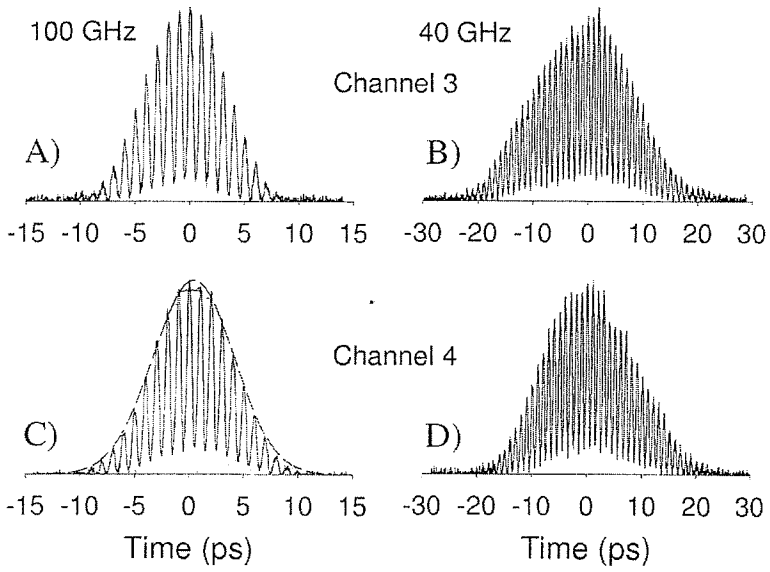


Fig. 2.3. Intensity corss-correlation of the output of both the 100 GHz channel spacing (left side A and C), and 40 GHz (right, B and D) on output channels 3 (top A and B) and 4 (bottom, C and D). Ref. Leaird et.al [1]

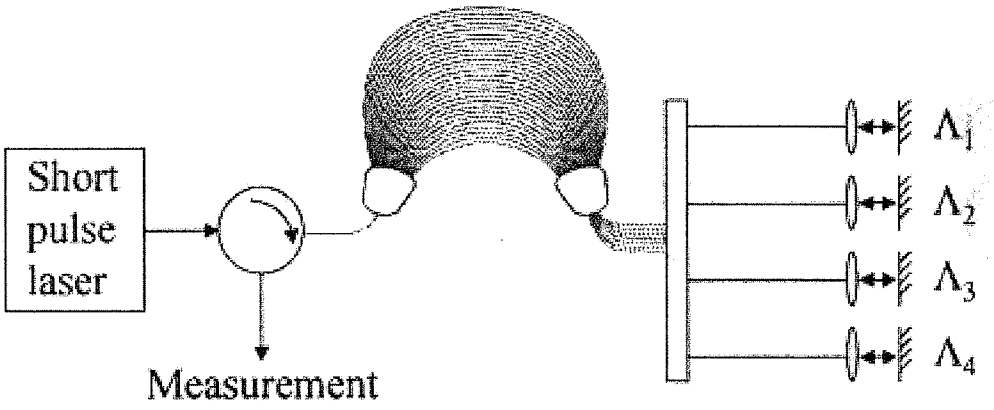


Fig. 2.4. Experimental set up of the double passed AWG. Ref. Leaird et.al [3].

### 2.2.1 A. Double pass experiments

The previous section described, what could also be called as a single pass configuration. An extension of this experiment would be to combine the various multiwavelength bursts at the each of the output waveguides with sufficient delay so that each train does not interfere with the other, and pass it again though the AWG. This time each train separately traverses through the waveguide array and undergoes further change in its temporal envelope (due to the fact that the AWG excitation profile is acted upon once again). All these 'time delayed and modified bursts' will combine to give a much larger and repeated pulse train, each pulse train being wavelength shifted (corresponding to each individual output waveguide on single pass). This configuration is the double pass configuration. A schematic diagram of the experimental set up of the double pass configuraton is shown in Fig. 2.3.

The following experiment [3] describes a double pass set up. Here the AWGs are engineered [8] so that the temporal envelope of the pulse train on single pass is flat (rather than Gaussian like). Each pass through the AWG can be modelled

as a finite impulse response filter (FIR) under suitable assumptions. More of this systems approach will be covered in the next chapter. Hence the output sequence is a convolution of the input pulse with its impulse response. Following this approach the a double passed set up is like a double convolution, or an autoconvolution. Now if we have a flat topped pulse train on single pass (a square envelope), the output of each pulse train on double pass would be a triangle (a well established convolution example in systems theory). The experiments in [3] were consistent with the theory. The ouput sequence recorded on double pass was a repeating triangular pulse train. A pattern of the output train is shown in Fig. 2.5. Thus the experiments in [1] and [3] have demonstrated the ability to generate complex optical waveforms over a large time window (of about 200ps) These investigations throw open the possibility of engineering a system that could potentially generate a flat topped train on double pass with a large temporal window (typically a few 100 pico seconds). This is precisely the design the present work is focused on.

## 2.3 The Problem Revisited

After discussions on the AWG and its newly explored functionality, it is now easier to state the design problem at hand and the engineering requirements:

1. To design an AWG through design to generate a flat topped pulse train on double pass. This design could be by varying the excitation profile and the phase difference between two consecutive waveguides, or vary the phase only. We shall see in the results section that both these possibilities have been explored. It would be better from the design perspective to choose the phase only approach.

2. The AWG system so designed should be robust within the limits of fabrication errors.

3. The AWG system should have a low insertion loss. Details of this parameter is covered in the next chapter.

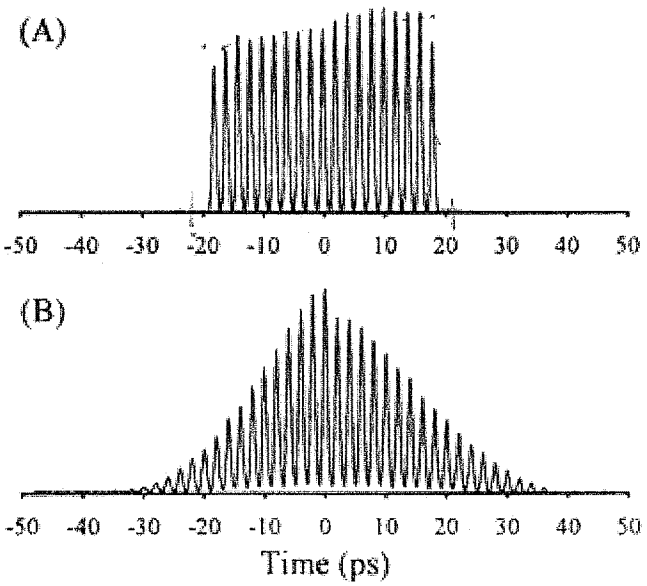


Fig. 2.5. a) Output from single pass. b) output from double pass. Ref. Leaird et.al. [3].

Having stated the problem clearly at this point of time, we proceed to the next chapter, in which the design approach is introduced in great detail.

# 3. MODELING AND OPTIMIZATION APPROACH

After understanding the basic working principles of the AWG, we now proceed to the details as to how the AWG can be treated as a Finite Impulse Response Filter (FIR filter). With the introduction to systems approach, we then proceed as to how the system requirements of this problem can be stated in terms of an optimization problem with various constraints. From this point onwards the AWG will be viewed as a FIR filter rather than an optical device. Most of the optics will now translate into systems theory and filter design. At the end of this chapter the problem will be restated as a filter design problem, to be solved using numerical optimization.

## 3.1 The AWG revisited: systems approach

The AWG device consists of three parts, a) The input waveguidefiber that acts as the input. b) The free propagation region (FPR) which is a slab waveguide followed by the waveguide array. The input electric field mode diverges in the slab waveguide and thus forms a kind of Gaussian spatial mode. This means that the central waveguides of the waveguide array receive greater amount of the energy than the ones away from the center. Each waveguide discretely receives a part of the energy, and this discrete set of values (proportional to the field amplitude collected per waveguide) is called as the excitation profile. Fig 3.1 is a schematic of the waveguide array section. Let us define the excitation profile in terms of coefficients $b_i$ where $b = [b_{-N}, \ldots, b_N]$. We choose an odd number of waveguides just for convenience of symmetry about the central waveguide. Each coefficient $b_i$ corresponds to the excitation of the $i^{th}$ waveguide, the waveguides being numbered from $-N$ to $N$, with the central waveguide being numbered as the $0^{th}$. It may be recalled from the previous chapter that this waveguide array is an optical delay line. Fig 3.1 depicts the fact that each waveguide has a

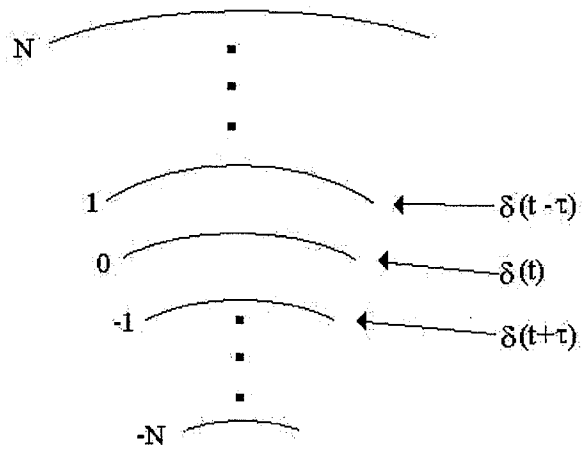


Fig. 3.1. A schematic of the waveguide array section.

particular delay associated with it corresponding to the length difference between two consecutive waveguides in the array. Also, the pulses in two consecutive waveguides can have a phase relationship with respect to each other. Therefore at the output end of the waveguide array, the electric field will undergo both delay and phase change with respect to the input. Thus neglecting dispersion, we can write the impulse response of the AWG device as:

$$h(t) = \sum_{j=-N}^{N} b_j \delta(t - j\tau) \tag{3.1}$$

where $h(t)$ is the impulse response, $\tau$ is the constant time delay between two consecutive waveguides. In this work, $\tau$ has been set to 1 ps. $\tau$ is varied by changing the physical lengths of the waveguides. Therefore the output electric field can be written as a convolution of the input electric field with the impulse response.

$$e_{out}(t) = e_{in}(t) * h(t) \tag{3.2}$$

where $e_{in}(t)$ and $e_{out}(t)$ are the input and output electric fields respectively, and h(t) is given by eqn. 3.1. '$*$' operation corresponds to convolution, as well understood in electrical engineering literature. Eqn 3.2 corresponds to a single pass through the device. On double pass, the combination of the mirror (Fig 1.2) and another pass through the device corresponds to another convolution. Hence the impulse response in double pass is an autoconvolution. In other words:

$$e_{out}(t) = e_{in}(t) * h(t) * h(t) \tag{3.3}$$

Note the fact that the input electric field is convolved with the impulse response being convolved with itself (auto convolution).

### 3.1.1 Frequency Domain

It is instructive to view Eqns 3.1 through 3.3 in frequency domain. The Impulse response in the frequency domain is given by the Fourier transform of equation 3.1:

$$H(\omega) = \sum_{m=-N}^{N} b_m e^{-jm\omega\tau} \tag{3.4}$$

here $j = \sqrt{(}-1)$ and thus Eqn. 3.3 reduces to:

$$E_{out}(\omega) = E_{in}(\omega)[H(\omega)]^2 \tag{3.5}$$

in the frequency domain. Using Eqn.3.4, with $z^m = e^{-jm\omega\tau}$ we can write $[H(z)]^2$ as:

$$[H(z)]^2 = \sum_{n=-2N}^{2N} a_n z^n \tag{3.6}$$

where $a_n$ is defined by:

$$a_n = \begin{cases} \sum_{k=-N}^{N+n} b_k b_{n-k} & \text{for } -2N \leq n \leq 0 \\ \sum_{k=-N+n}^{N} b_k b_{n-k} & \text{for } 0 < n \leq 2N \end{cases} \tag{3.7}$$

In other words the $a_n$'s represent the discrete values of the auto-convolution at times equal to a multiple of $\tau$, or the amplitude profile of the pulse train so formed due to double pass through the AWG.

## 3.2 Filter Design

We saw in Eqn. 3.7 that it is easy to represent the double pass discrete temporal envelope through the discrete autoconvolution sequence, $a_n$. This means that we can set a value equal to the pulse height at every value of $a_n$, to represent the pulse train. Our aim now is to generate that set of filter coefficients $b_m$ such that on convolution the sequence $a_n$ (which is a function of $b_m$ due to Eqn. 3.7 ) represents a square window (flat topped) in time domain. Or, we need to generate a set of pulses that have a similar height and the rest of them going to zero, (thus representing a square). This condition can be mathematically stated as follows:

$$a_n = \begin{cases} A & \text{for } -l \leq n \leq l \\ 0 & \text{otherwise} \end{cases} \tag{3.8}$$

Where $A$ is the electric field amplitude on double pass. $l$ decides the number of pulses we want and the total number of $a_n$'s is related to the number of waveguides present in the AWG. Our filter design is in terms of the complex filter coefficients $b_m$'s. Thus we can think of a few possible ways to design based on this:

### 3.2.1 Unconstrained filter

The amplitude profile of the filter coefficients actually represents the excitation profile, that can be fabricated using loss-engineering of AWGs [8]. However a random amplitude/excitation profile would be really difficult to fabricate. Besides, as we shall see in the next chapter, this loss engineering would add extra insertion loss to the system. This is rather undesirable. The phase profile means that the physical length of the waveguides is tailored such that extra phase (apart from a multiple of $2\pi$ due to the preset time delay) is accumulated in every waveguide as dictated by the profile. Thus the unconstrained optimization means that we seek a design in terms of both phase and amplitude engineering.

### 3.2.2 Phase only filter

In this approach the amplitude profile is kept constrained most likely to the naturally occuring Gaussian. This means that our design will only have phase profile. From the fabrication point of view, this means that the physical length of the waveguides is the only parameter that needs to be taken care of. At the outset it seems very clear that the phase only approach is rather more acceptable from a practical point of view. Besides the present fabrication techniques [12] easily have a precision of forty to fifty parts of a wavelength. Nevertheless most of the design proposed in this work will be based on the phase only approach. It will be seen that this approach yeilds very good results, even after taking into account possible fabrication errors. However a small part of the next chapter will also cover the unconstrained approach as a demonstration, in order to elucidate the optimization approach [10-11].

## 3.3 Problem Statement

Our design problem is stated in a way that the design paramenters returned are the filter coefficients (both amplitude and phase). Just as in any optimization problem, we have an objective to be minimized and the rest of our requirements act as constraints to the problem. In our case the objective function has to do with the fact that we require a square pulse in time domain. This requirement means that the output electric field (on double pass) is almost equal to a constant value for some pulses and is almost equal to zero for the rest of them. So we can define tolerances $\epsilon$ such that:

$$\Big|\, |\, e(t)\, | - A \Big| \leq w\epsilon \qquad \text{for} - T_{sq} \leq t \leq T_{sq} \tag{3.9}$$

$$|\, e(t)\, | \leq w\epsilon \qquad \text{otherwise} \tag{3.10}$$

Where $|\, e(t)\, |$ denotes the electric field amplitude on double pass (or pulse amplitude height) and $T_{sq}$ in the time domain denotes the extent of the square. $\epsilon$ is a scalar denotes the tolerance from the actual value, and $w$ is a vector that decides the relative

weights that different functions are subjected to. For example, we would set a greater weighting coefficient in the region defined in Eqn 3.9 to have a flatter pulse. Having defined this, its easy to translate this to the case of discrete pulses, knowing that we want $2l+1$ pulses having an amplitude of $A$ and the rest going to zero. Remember from Eqn.3.7, that the amplitude of each pulse in the double pass convolution is given by $a_m$, which in turn is a function of the filter coefficients:

$$F_n(b_i) = \begin{cases} \Big|\,|\,a_n\,| - A\Big| & \text{for } -l \leq n \leq l \\ \Big|a_n\Big| & \text{otherwise} \end{cases} \tag{3.11}$$

This set of functions form the multiobjective objective function to be minimized. So the formal optimization problem statment is:

$$\text{minimize} \quad \epsilon \qquad \text{such that} \quad F_n(b_i) \leq w.\epsilon \tag{3.12}$$

where $F_n$ is the vector objective function defined in Eqn. 3.12.

### 3.3.1 Filter Amplitude Constraints

The most naturally occuring amplitude profile in the AWG is a Gaussian. Hence it is useful for us to constrain the amplitude profile of the filter coefficients to be Gaussian. This means that the excitation is maximum at the central waveguides and falls off on both sides of the central waveguide. The function used to set this constraint is as follows:

$$b_m = b_0 e^{-\frac{m^2}{b_w{}^2}} \tag{3.13}$$

where $b_w$ decides the width of the Gaussian profile. Hence with this as the constraint we only have the phase profile of the waveguides as the degree of freedom in our design.

### 3.3.2 Spectral constraints and Insertion loss

So far the constraints placed have been totally in the time domain, the fact that we require flat topped pulse and also the amplitude/excitation profile constraint. But

we have a few additional requirements for a realistic device. The requirement is that our design also incorporates a minimum insertion loss. This requirement stems out as a spectral constraint. We shall soon see how.

The insertion loss is simply defined as the ratio of the output to the input power. This device is a double pass arrangement, which implies that spectral power which is discretely received by the output waveguides is again routed back through the waveguide array into the input waveguide. The possible mechanism of insertion loss is the amount of power that leaks out in the receiver section. In other words if more energy can be concentrated into the output waveguide, we are guaranteed of lesser insertion loss. Usually, insertion loss is determined through experiments. However, based on the explanation given above, we have a mathematical formulation of insertion loss. We determine insertion loss with respect to a standard device. The standard device here is the AWG with the same Gaussian amplitude profile as the design, but with no specially tailored phase profile, that is with real filter coefficients. The reason for insertion loss is therefore spectral distortion due to the phase profile. Fig. 3.2(a) shows a the Gaussian excitation profile in time domain, with each waveguide mapping to the delay in (ps). Zero delay is the central waveguide and so on. The waveguides with positive time delay are the longer ones and the waveguides with negative delay are the shorter ones. Fig. 3.2(b) shows the correpsonding power spectrum. Fig. 3.2(c), shows a phase profile applied to each waveguide and Fig. 3.2(d) shows that the power spectrum has changed quite a bit. Since the device is double passed we can define the ratio of the output powers of the two devices. This is done by discretely summing up the energies due to each output waveguide. This amounts to how much of the energy from each output waveguide has been directed back into the input on double pass. We perform a summation of the individual energies because we have a sufficient delay line attached to each output waveguide so that there is no interference between the energies in the output waveguides. Next we assume that the spectral profiles of each of the output waveguide is identical but only frequency shifted. Finally, assmuming that the input spectrum is much broader than the FSR, we can easily show that the

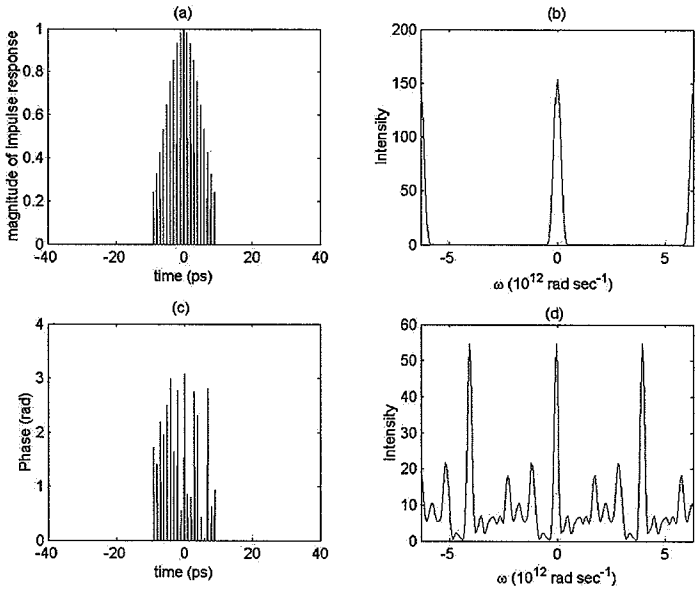


Fig. 3.2. a) Gaussian AWG filter coefficients (magnitude). b) Power Spectrum. c) Tailored Phase profile. d) Power spectrum after Phase profile is included in (a).

ratio of ouput energies of the phase modulated device and the standard device is given by:

$$P_r = \frac{\int_{-\pi}^{\pi} \mid H(\omega) \mid^4 d\omega}{\int_{-\pi}^{\pi} \mid H_0(\omega) \mid^4 d\omega} \tag{3.14}$$

Where $H_0(\omega)$ and $H(\omega)$ are the power spectra of the standard AWG and the Phase only AWG respectively. Since the spectrum is periodic, the energy in one FSR is used for evaluating it. Now the insertion loss is:

$$I_{loss} = 10log(P_r) \tag{3.15}$$

Thus we have seen how insertion loss manifests as a spectral constraint. We need to incorporate this into the optimization problem as a constraint. Note that more energy confined in the region of the output waveguide, results is lower insertion loss. This means that our spectrum must have a concentration of energy around the central

frequency. We shall call this small band of frequencies close to the central frequency of each waveguide as the in band. This means that, we can formulate the constraint in order to maximize the energy inside this 'inband'. The width of this band is decided based on the in-band width that corresponds to a 10 dB width in the standard AWG. This happens to be roughly in the order of $\frac{\pi}{3} \times 10^{12}\ rad\ sec^{-1}$. Now we are in a position to formulate this constraint as:

$$\int_{out-band} \mid H(\omega) \mid^2 d\omega \leq \alpha . \int_{in-band} \mid H(\omega) \mid^2 d\omega \tag{3.16}$$

This constraint guarantees that a small fraction ($\alpha$) of the total is contained outside the inband. The limits of the integral are set based on the inband and out band widths.

It is now intutive that as $\alpha$ is gets small, we have a sharp peaking of energy inside the in-band. This, of course leads to the fact that the ratio of the integrals in Eqn. 3.15 tends to 1, which inturn results in decreasing the insertion loss. However we shall see in the next chapter that there is a trade-off between the time and frequency domain. As we perform better in terms of insertion loss (by setting lower values for $\alpha$), we tend to perform poorer in time domain. The flat topped pulse tends to develop more power in the wings, consequently losing its square characteristic. This trade-off will be covered in great detail while summarizing the results.

### 3.4 The optimization

The optimization problem formulated is a nonlinear multiobjective optimization problem. It has been solved numerically using the optimization tool box of MATLAB. The function used here is the fminimax, which uses the Sequential Quadratic Programming (SQP) optimization approach applied to multiobjective optimization [9],[10]. This function works with complex filter coefficients. the filter coefficient $b_i$ is represented as a complex variable.

$$b_i = x(i,1) + jx(i,2) \tag{3.17}$$

where $x$ is an $N \times 2$ array whose entries correspond to the real and imaginary parts of $b$, and $j = \sqrt{(-1)}$. Both the objective function and the constraints are written as functions of $x$. Another important thing is how the weights are set. The weights are set up in the objective function. Depending on how much variation is allowed in the square part, we attach a greater amount of weight to the elements of this array that correspond to the pulse heights of amplitude $A$. A typical weight vector would be:

$$w_n = \begin{cases} w_1 & \text{for} - l \leq n \leq l \\ 1 & \text{otherwise} \end{cases} \tag{3.18}$$

Where $w_n$ is the weight array. Based on the formulation of the objective in Eqn 3.12 $w_1 < 1$ ensures that a greater weight is assured for the $2l + 1$ pulses with height $A$. For example, setting $w_1 = 0.01$ ensures that there is only about 1 percent variation in the wings. The MATLAB code accepts an initial guess value of the filter coefficients, the number of waveguides $2N + 1$, the number of pulses $2l + 1$, and the width of the time window. The optimization terminates with appropriate filter coefficients, using which we can plot the various results. Having understood this we are now in a position to discuss the so obtained results and designs.

# 4. RESULTS

So far, various aspects of our design has been presented. This chapter will discuss the results in great detail. The course of this chapter is as follows. First, design based on unconstrained optimization will be presented in order to elucidate various aspects of the result. Next, design based on the spectral and amplitude constraints discussed earlier is presented. Alongside, we also present the trade off curves so that an optimum design based on the system requirements can be picked. A design which is picked up from the optimum curves is analyzed for its robustness.

## 4.1 Unconstrained Optimization

As discussed at the end of the previous chapter, the optimization problem is solved using the minimax optimizer in MATLAB [9]. In our design, we come up with a set of filter coefficients $b_i$. The output temporal profile is obtained by autoconvolution of the FIR filter impulse response whose coefficeints are the $b_i$'s. This temporal profile is actually the product of double passing from one output waveguide. Recall that, we expect similar pulse trains in the other output waveguides too, except the fact that they are shifted in wavelength . These are combined after sufficient delays (as shown in Fig. 1.2), so as to combine them without overlapping. Thus it is enough, to show simulation results that depict the case of one such pulse train. Without loss of generality, we choose the central output waveguide (the waveguide that corresponds to the central frequency of the input pulse). A few other important aspects of the simulation are:

1. The number of waveguides in the Array. This can be adjusted as per requirements. We have used a standard of 19 waveguides in most of the simulations.

2. The number of pulses per output waveguide/channel. This can also be set accordingly in the object function of the optimization problem. We have used 11 as the number of pulses.

3. Relative weights are assigned to the objective function. We set weights depending on our requirements with respect to the final temporal response, depending on how much variation is allowed in the flat topped envelope, relative to the wings.

In case of unconstrained optimization, we allow both amplitude and phase to vary freely, thus adding to the degrees of freedom for our design. Added to this we do not have any spectral constraints. Hence the problem is just to find the local minimizer for the objective function. Hence the optimization problem has the following form:

$$\text{minimize} \qquad F_n(x) \qquad n = 1, \ldots, q, \tag{4.1}$$

Where $F_n(x)$ is the set of multiobjective functions (in our case the given by Eqn. 3.12). This would set the pulse heights close to one for $-l \leq n \leq l$ and zeros elsewhere. The design will hence be the filter design coefficients $b_i$'s. With these coefficients, we would have to perform loss engineering [8] to engineer this amplitude profile, and also vary the lengths of waveguides with precision to tailor the phase. Fig. 4.1 shows an elementary design. Both amplitude and phase profile is shown. Fig. 4.1(c), (d) shows the output temporal profile (intensity, obtained as the magnitude squared of the electric field) and the power spectrum respectively. It is observed that the output temporal profile is almost perfectly a square. Besides this, we note that the spectrum is highly jagged, and based on our formulation of excess insertion loss (Eqns. 3.14-3.15), it was calculated to be 14.92 dB. This is quite a poor design, although we get an excellent temporal profile. However, it was highly instructive to begin the quest for a good design with a flavor of unconstrained optimization. These results were displayed in order to illustrate some important aspects of the problem. The next section is devoted to the discussion of the results of constrained optimization.

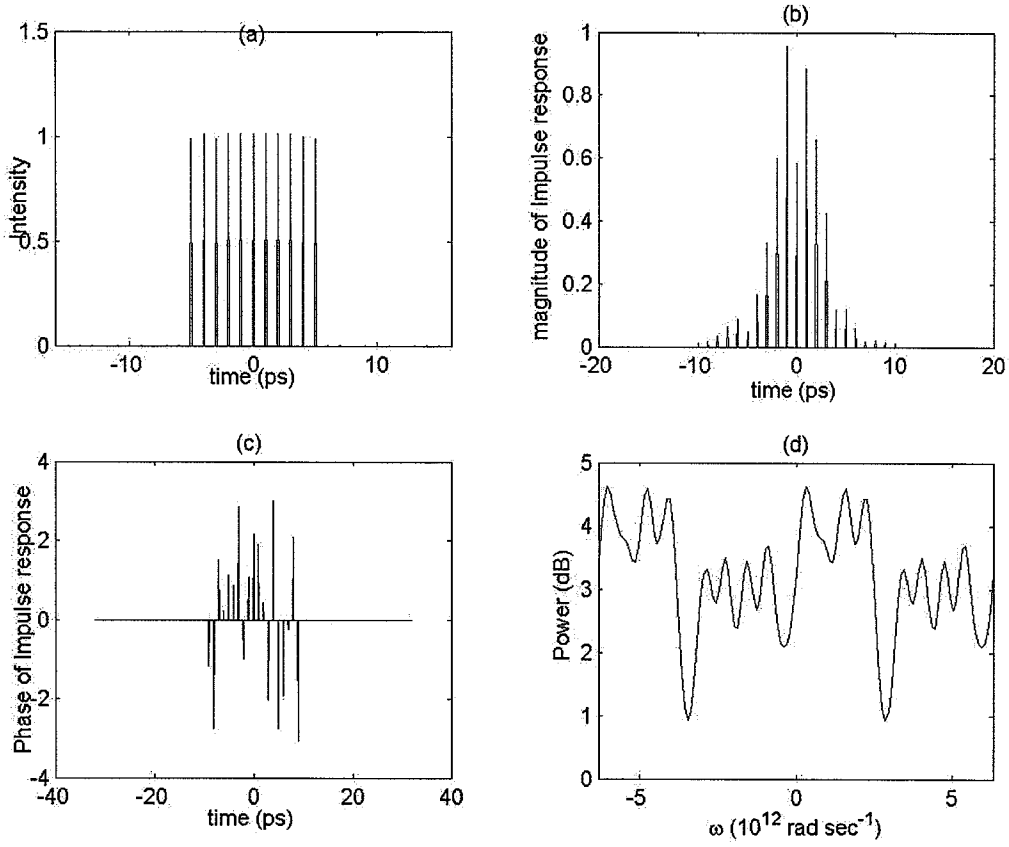


Fig. 4.1. a) Output Intensity profile. b) Filter Amplitude coefficients (excitation profile of the AWG). c)Phase profile. d) Power Spectrum of the AWG.

## 4.2 Constrained Optimization

In the end of the previous chapter, the concept of constrained optimization applied to our work was introduced briefly. There are several important factors that come to play while coming up with designs to meet specific conditions. The following sub-sections will discuss most of them in detail. The next section will then introduce the concept of trade-off curves, that will elucidate how to select a optimum design based on specific criteria.

### 4.2.1 A. Constraint on the Amplitude

We are to design a phase only filter, with the amplitude profile restricted to be a Gaussian. Having decided the number of pulses per channel, and the number of waveguides in the array, it is important to decide on the width of the Gaussian function that the filter (Eqn. 3.14) will assume. In all the simulations, we have chosen 11 pulses per channel, and 19 waveguides in the array. The results can be extended for any number of pulses with appropriate number of waveguides in the array. With a fixed number of waveguides in our design, we can set the width of the Gaussian usually in the order of the number of waveguides in each side of the central waveguide. With an odd choice of the number of waveguides in the array $N$, it is clear that there are $\frac{(N-1)}{2}$ waveguides on both sides. Therefore a choice in the order of $\frac{(N-1)}{2}$ would be a good choice for the width parameter $b_w$ in Eqn 3.13. Fig 4.2(a) (b) shows the effect of adjusting $b_w$. Two choices considered here are $b_w = \frac{(N-1)}{4}$ and $b_w = \frac{(N-1)}{2}$. It is seen that the energy in the wings in Fig 4.2(a) is much lesser. Increasing the width causes more energy in the wings, probably as a result of double convolution. Intutively it is probably true that the width $b_w$ must be chosen such that the convolution of the Gaussian with itself expands over a temporal window close that in the order of the number of pulses required. In these plots the weight function was set so as to allow very small variation to the square envelope. The results shown here and henceforth are typical, after observing the trend when the optimization code

is run for several iterations (usually around 25-30). The optimum width in chosen in our case is $0.35(N-1)$, which is somewhere between the two cases considered here. This choice was determined using several trials of Gaussian widths. However this choice depends on the relationship between $N$ and $L$ (the number of pulses per channel).

### 4.2.2 Spectral Constraints

Spectral constraints have been discussed in the previous chapter. Minimizing insertion loss seems to be the other concern. Based on the discussion in section 3.3.2, the insertion loss is estimated as an excess insertion loss with respect to the standard AWG device (without phase modulation). This parameter is indirectly controlled as a constraint in Eqn 3.17, in which we try to maximize the energy contained inside the in-band. This would give the spectrum a peaked character. A peaked spectrum would minimize the excess insertion loss, because we are evaluating this as a ratio ($P_r$ in Eqn 3.15) with respect to a well peaked spectrum $\mid H_0(\omega) \mid^4$. $\alpha$ is the parameter controlling the amount of energies contained inside and outside the in-band. Plots in Fig. 4.3 show the effect of $\alpha$ on the nature of the temporal profile. These plots are again generated with the weight functions set so as to have very less variation in the square part of the envelope. Firstly, orders of $\alpha$ map directly to the insertion loss value. These have been mentioned in the plots. There exists trade-off between insertion loss value and how good the flat topped output is. We can see from the plots that as the excess insertion loss decreases ($\alpha$ tending to 0), the output pulse train begins to devlop greater energy in the wings, besides beginning to lose flatness. This is probably because as the excess insertion loss tends to zero, the spectral features will more and more resemble that of the standard Gaussian (as seen comparing Fig 4.4(a) and (d)), and hence we will have to compromise on the quality of the flatness in time domain. Therefore, from the plots it is clear that for $\alpha \sim 0.45$, corresponding to an excess insertion loss of about 4.5-5 dB, the temporal output seems to be fit well

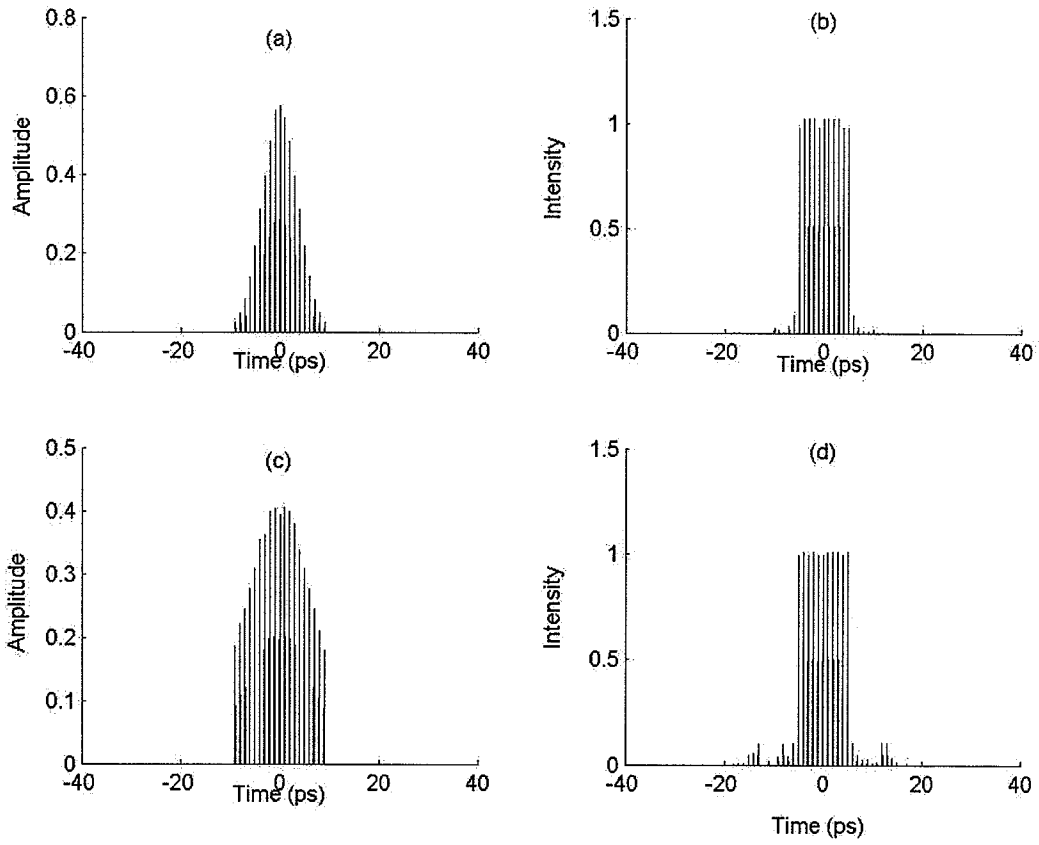


Fig. 4.2. Effect of the width of the Gaussian filter: a) Gaussian Filter of Width $b_w = \frac{(N-1)}{4}$. b) Output pulse train on double pass. c) Gaussian Filter of Width $b_w = \frac{(N-1)}{2}$. d) Output pulse train on double pass.

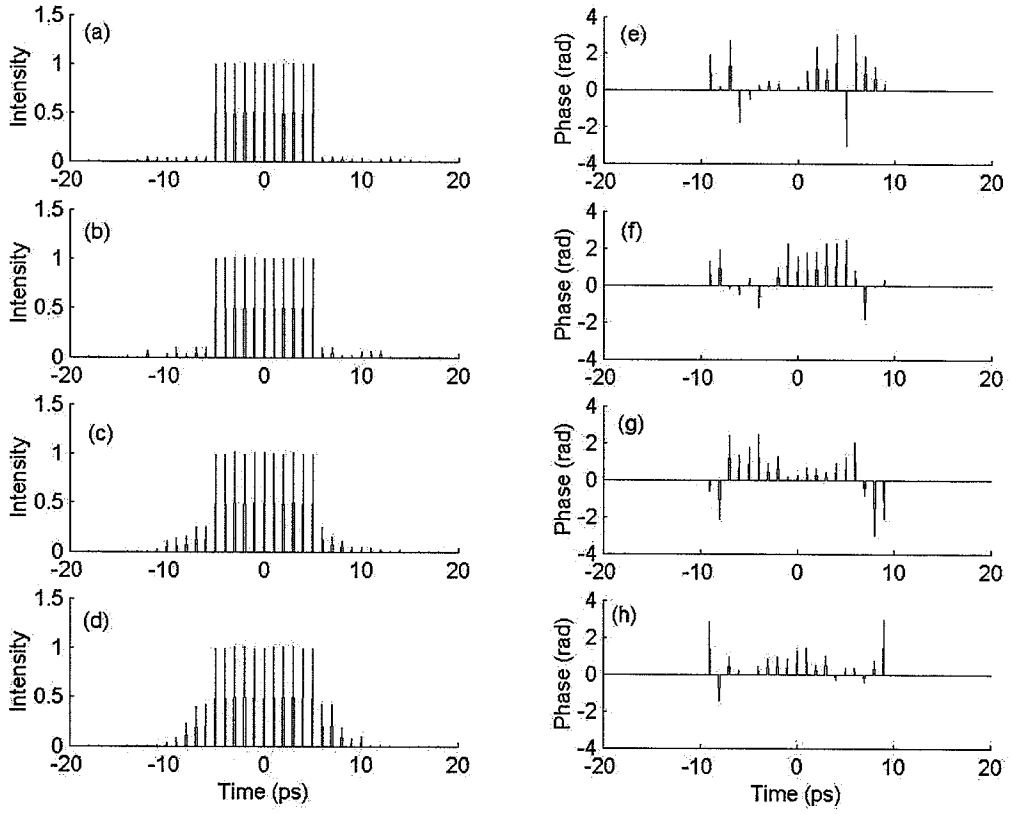


Fig. 4.3. Examples of output temporal and phase profiles for various values of $\alpha$. (a)$\alpha = 0.45$ (b)$\alpha = 0.35$ (c)$\alpha = 0.25$ (d)$\alpha = 0.15$

into our criteria. We are now on our way to pick up an optimum design. For now, we have fixed the following:

1. The width of the Gaussian filter $b_w$.

2. The value of $\alpha$, order of excess insertion loss, based on comparative plots.

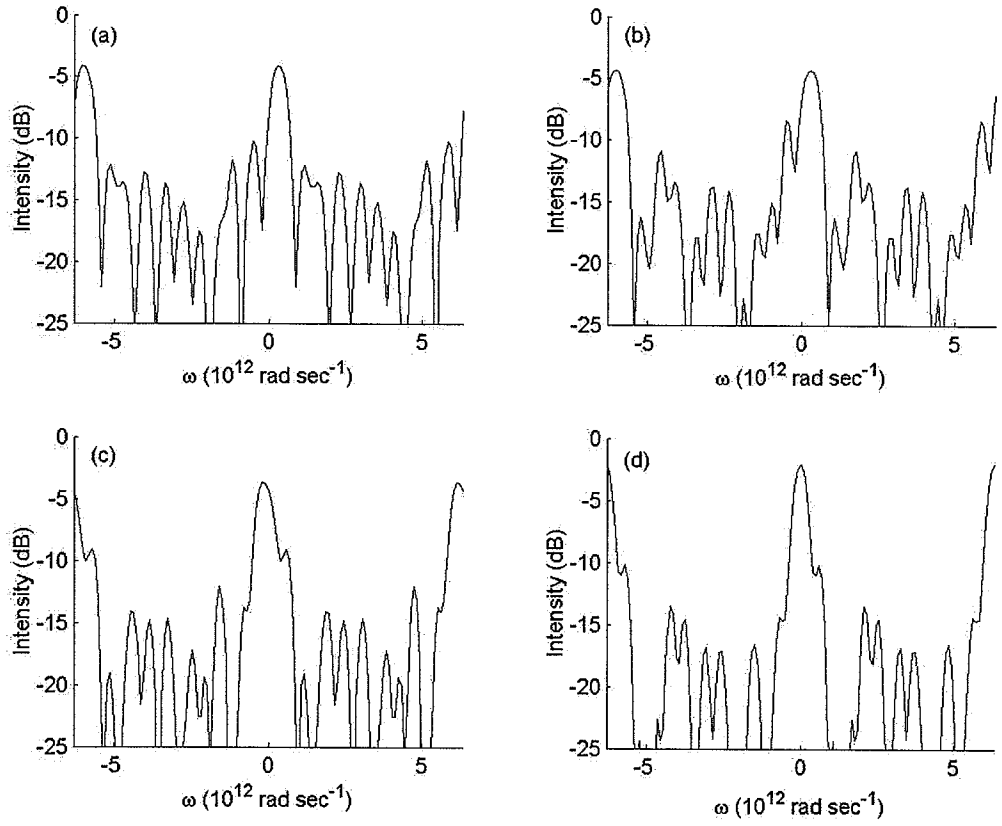


Fig. 4.4. Examples of output Normalized spectral profiles for various values of $\alpha$. (a)$\alpha = 0.45$ (b)$\alpha = 0.35$ (c)$\alpha = 0.25$ (d)$\alpha = 0.15$

Table 4.1
Table of calculated excess insertion loss for different values of $\alpha$

| $\alpha$ | Insertion Loss (dB) | Peak Insertion Loss (dB) |
|---|---|---|
| 0.15 | 0.87 to 1.05 dB | 1.2 dB |
| 0.25 | 1.77 to 1.89 dB | 2.1 dB |
| 0.35 | 3.08 to 3.22 dB | 3.6 dB |
| 0.45 | 4.33 to 4.52 dB | 4.8 dB |

### 4.2.3 Insertion Loss

As mentioned earlier, the relative excess insertion loss is calculated based on the formulation in Eqn. 3.14. Fig. 4.4 shows the different spectra corresponding to different orders of $\alpha$. The spectrum is calculated on a dB scale normalized with respect to the standard AWG device. Peak excess insertion loss is the difference between the $0dB$ mark and the peak of the spectrum. For example in Fig. 4.4 (a) that this is found to be $4.8dB$ whereas in Fig. 4.4(d), it is found to be $1.2dB$. In other words, the peak of the spectrum rises closer to the $0dB$ mark as we decrease the value of $\alpha$ (or increase the amount of energy inside the in-band). Table 4.1 shows the range of calculated values (from Eqn. 3.14) of excess insertion loss against corresponding values of $\alpha$, showing that there is more insertion loss as lesser energy is confined in the inband. The Peak Insertion loss is a measure that is simply the distance of the spectral peak from the 0 dB mark in the normalized spectral proflile plot in Fig. 4.4.

### 4.2.4 Time Domain: What is acceptable?

The next question that comes to mind is, what is a good measure to quantify a flat topped pulse, alternatively, how do we pick a particular square envelope over the

other?. An answer to this question will complete most of our questions on the design criteria. The following qualitatively measures a 'good' square envelope:

1. The intensity fluctuations about a constant value within the square time window must be small.

2. The intensity fluctuations in the region ouside the square time window (the wings) must be small.

Based on this, we can decide on two quantities $W_1$ and $W_2$, which are defined as the maximum intensity fluctuation within the square and in the wings respectively. Based on the weights $w$ set on the optimization parameters, we can increase $W_1$ to decrease $W_2$ and vice versa. A detailed study of this idea will be done in the next section.

### 4.3 Selection of the optimum design: Tradeoff curves

We now need to take a better look at the time domain. At the outset it seems that we need temporal envelopes that fall to zero sharply, besides maintaining a minimum fluctuation in the wings, even if this could be acheived with a small variation in the square region of the pulse. Having stated this, we pick our design based on trade off curves.

#### 4.3.1 Trade-off analysis

Our problem is a multiobjective optimization problem [11] which is of the form

$$\begin{aligned} \text{minimize} \quad & F_n(x) \qquad n = 1, \ldots, q, \\ \text{subject to} \quad & g_i(x) \leq 0, \quad i = 1, \ldots, m \\ & h_i(x) = 0, \quad i = 1, \ldots, p \end{aligned} \tag{4.2}$$

where $F_n(x)$ is the set of multiobjective functions (in our case the given by Eqn. 3.11), $g_i$ and $h_i$ are the inequality and equality constraint functions (Eqns 3.16, 3.13

respectively). When there is an optimum point, we say that the objectives are non-competing, since there is no compromise made among the objectives.

A Pareto optimal point $x^{po}$ satisfies the following: if $y$ is feasible and $F_i(y) \leq F_i(x^{po})$ for $i = 1, \ldots, q$. then $F_i(x^{po}) = F_i(y), i = 1, \ldots, q$. This can be restated as: If a feasible point is not Pareto optimal [11], there is at least one other feasible point that is better. In trade-off analysis we consider Pareto optimal points. Let us consider $x$ and $y$ as Pareto optimal points.Let A be a set of objectives for which $x$ beats $y$, B is the set of objectives for which the points $x$ and $y$ are tied, and C is the set of objectives for which $y$ beats $x$. If A and C are empty, then the two points $x$ and $y$ have exactly the same objective values. If this is not the case, then both A and C must be nonempty. Therefore, the idea behind two Pareto points is that they either perform equally or each beats the other in at least one objective. In comparing points $x$ and $y$, we say that we have traded off better objectives in set A and worse objectives in set C. Therefore, in our trade-off analysis we consider how the maximum deviation in the wings $W_2$ is traded off with the maximum deviation within the square $W_1$. Further, we now define $W_1$ and $W_2$ as

$$W_1 = \max \mid\mid e(t) \mid^2 -1 \mid \qquad \text{for} - T_{sq} \leq t \leq T_{sq} \tag{4.3}$$

$$W_2 = \max \mid e(t) \mid^2 \qquad \text{otherwise} \tag{4.4}$$

where $T_{sq}$ denotes the extent of the square envelope. $\mid e(t) \mid^2$ denotes the intensity of electric field, which has been set to 1 for our simulations. Before beginning the next subsection, we summarize the trade-offs in our analysis

1. The relative intensity fluctuation in square and in the wings. We require to minimize both for a decent flat toppped envelope.

2. Spectral constraints: Excess insertion loss in (dB) maps directly to the amount of energy in the inband (table 4.1). Good flat topped envelopes have a lower value of $\alpha$ and consequently a higher insertion loss.

Therefore we increase our excess insertion loss in pursuit of a better flat topped envelope.

### 4.3.2 Trade-off curves: Selection of an optimum solution

Based on the explanation above, we construct trade-off curves, for different orders of insertion loss. These curves will be parallel curves. We construct the trade-off curves by choosing closely spaced optimal points. Each optimal point has been set by a weight vector that adjusts the values $W_1$ and $W_2$. The trade-off curve is plotted with $W_2$ as the x-axis and $W_1$ as the y-axis. Since the optimizer is a local optimizer, the program is run for 50 iterations to find the closest point to the origin, for each set of weights chosen. Each iteration begins with a random guess design. Fig 4.5 shows a set of trade off curves, for different orders of insertion loss. Notice that the curve shifts closer to the origin, which means better performance for a square envelope, as the insertion loss increases. The two points marked (a),(b) are the closest to the the x-axis, and hence represent designs with very little fluctuations of intensity. Notice that the variation in the wings is much lesser than the variation in square (easily seen noticing the x and y axes). This means that in order to gain a little better performance in the wing area, we have to trade-off heavily in the square region. The point (d) represents the point farthest from origin and thus will have a violent variation in its temporal envelope. Fig 4.6 and 4.7 show the various designs corresponding to these points. Fig. 4.8 shows the corresponding temporal profiles. Notice that designs (a) and (b) represent quite well behaved square envelopes, with little variation in the envelope. Design (c) shows about 10 percent variation in the square region, and (d) shows about 15-20 percent. Hence it can be seen that these curves are extremely useful to pick up quality designs. If we were to implement some of these designs, we would require to know the phase values precisely. This would correspond to the extra path length that has to be added or subtracted (depending on the sign of the phase) from the standard delay length. Tables 4.2-4.5 show the phases calculated for the designs of (a) through (d) from the trade off curves. Note that the 19 waveguides are numbered from $-9$ to 9. Table 4.6 shows the calculated excess insertion loss for the

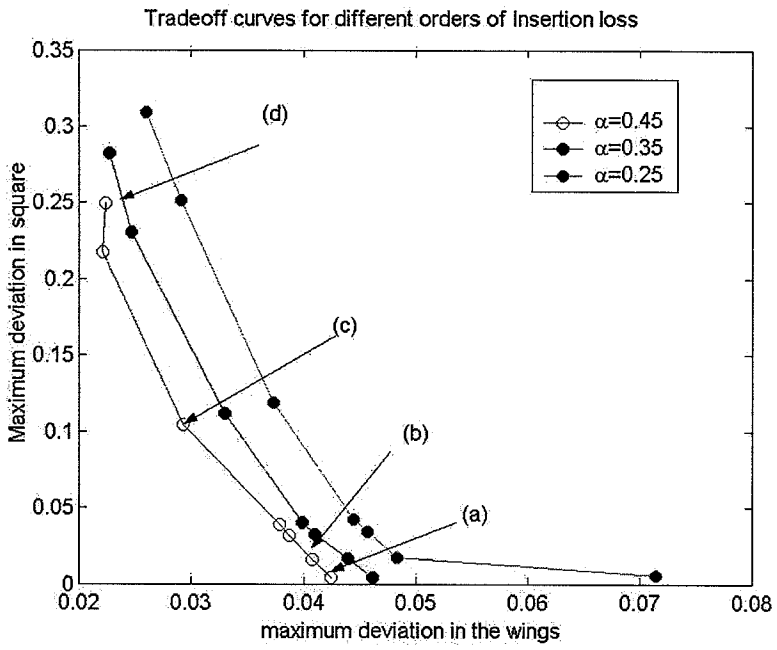


Fig. 4.5. Trade-off curves for different values of $\alpha$/ insertion loss.

designs. We see that these designs (corresponding to all the points on the trade-off curve for $\alpha = 0.45$) have a mean insertion loss of 4.45 dB.

## 4.4 Robustness

Any good design must be tolerant to fabrication errors. The error that could be deliterious to this system is the phase error in the waveguide array. State-of the art experimental techniques [12],[16] have been developed such that path length jitters due to fabrication errors occur in the order of usually around a 25th of a wavelength.

Table 4.2
Table of Phase v/s Waveguide number for design (a)

| Waveguide number | Phase (rad) |
|---|---|
| -9 | 1.8816 |
| -8 | 0.1516 |
| -7 | 2.7055 |
| -6 | -1.7231 |
| -5 | -0.4660 |
| -4 | 0.2585 |
| -3 | 0.2585 |
| -2 | 0.5105 |
| -1 | 0.3170 |
| 0 | -0.3340 |
| 1 | 0.1890 |
| 2 | 1.0141 |
| 3 | 2.3484 |
| 4 | 1.1198 |
| 5 | 3.0449 |
| 6 | -3.0504 |
| 7 | 2.9844 |
| 8 | 1.8611 |
| 9 | 0.3239 |

Table 4.3
Table of Phase v/s Waveguide number for design (b)

| Waveguide number | Phase (rad) |
|---|---|
| -9 | 0.6962 |
| -8 | 0.1128 |
| -7 | -1.0319 |
| -6 | -1.2613 |
| -5 | -1.0772 |
| -4 | 0.8522 |
| -3 | -0.3858 |
| -2 | 0.9404 |
| -1 | 1.7695 |
| 0 | 1.9957 |
| 1 | 1.6502 |
| 2 | 1.4593 |
| 3 | 1.7336 |
| 4 | 2.4788 |
| 5 | -2.4854 |
| 6 | -0.7176 |
| 7 | 1.9137 |
| 8 | 0.0821 |
| 9 | -0.3858 |

Table 4.4
Table of Phase v/s Waveguide number for design (c)

| Waveguide number | Phase (rad) |
|---|---|
| -9 | 0.7096 |
| -8 | -1.5035 |
| -7 | 1.5501 |
| -6 | 3.0702 |
| -5 | -1.6581 |
| -4 | -0.8349 |
| -3 | -0.5685 |
| -2 | -0.7613 |
| -1 | -1.0953 |
| 0 | -0.8048 |
| 1 | -0.0391 |
| 2 | 1.3014 |
| 3 | 0.0635 |
| 4 | 1.9158 |
| 5 | 2.1948 |
| 6 | 2.0052 |
| 7 | 0.5942 |
| 8 | 0.3605 |
| 9 | -0.8790 |

Table 4.5
Table of Phase v/s Waveguide number for design (d)

| Waveguide number | Phase (rad) |
|---|---|
| -9 | -0.6042 |
| -8 | 1.9359 |
| -7 | 2.9135 |
| -6 | 0.4109 |
| -5 | -1.3944 |
| -4 | -1.2072 |
| -3 | -2.0863 |
| -2 | -0.9758 |
| -1 | -1.1423 |
| 0 | -0.9642 |
| 1 | -1.3623 |
| 2 | -0.3045 |
| 3 | 0.8986 |
| 4 | 1.4128 |
| 5 | 0.1729 |
| 6 | 1.5167 |
| 7 | -0.5026 |
| 8 | -2.1546 |
| 9 | -0.2556 |

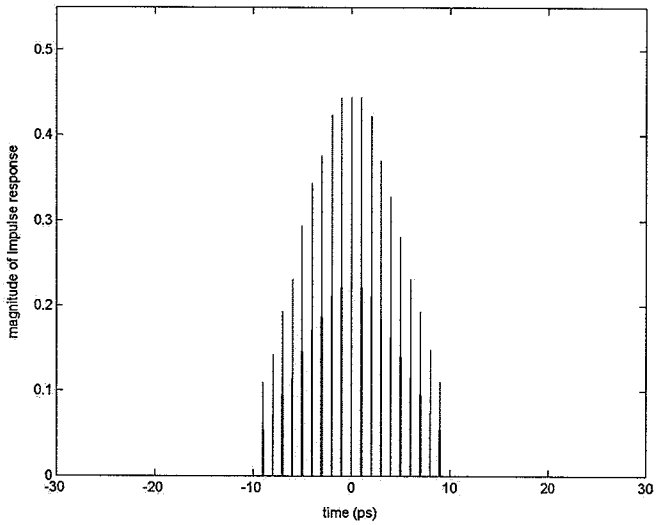


Fig. 4.6. Amplitude Profile of the Design.

Table 4.6
Table of calculated excess insertion loss for designs (a), (b), (c) and (d) on the trade-off curve for $\alpha = 0.45$

| Design | Insertion Loss (dB) |
|---|---|
| (a) | 4.33 dB |
| (b) | 4.35 dB |
| (c) | 4.43 dB |
| (d) | 4.52 dB |

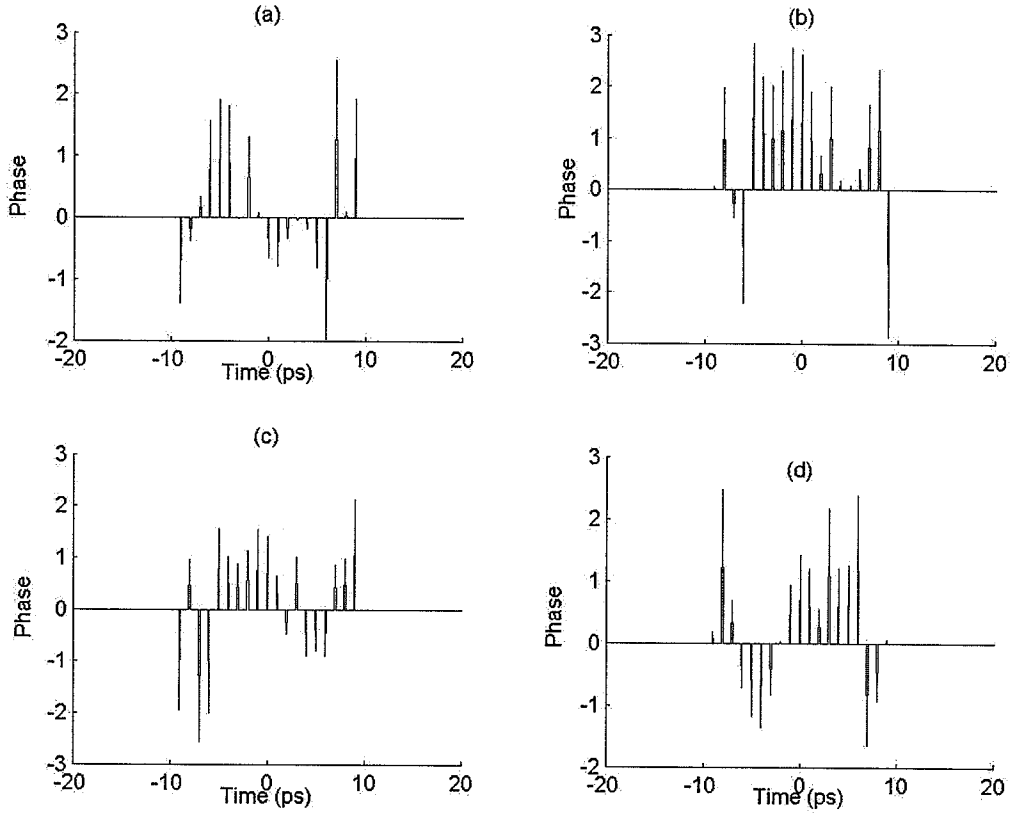


Fig. 4.7. Phase profiles of the design, corresponding to points (a), (b), (c) and (d) on the trade-off curve.

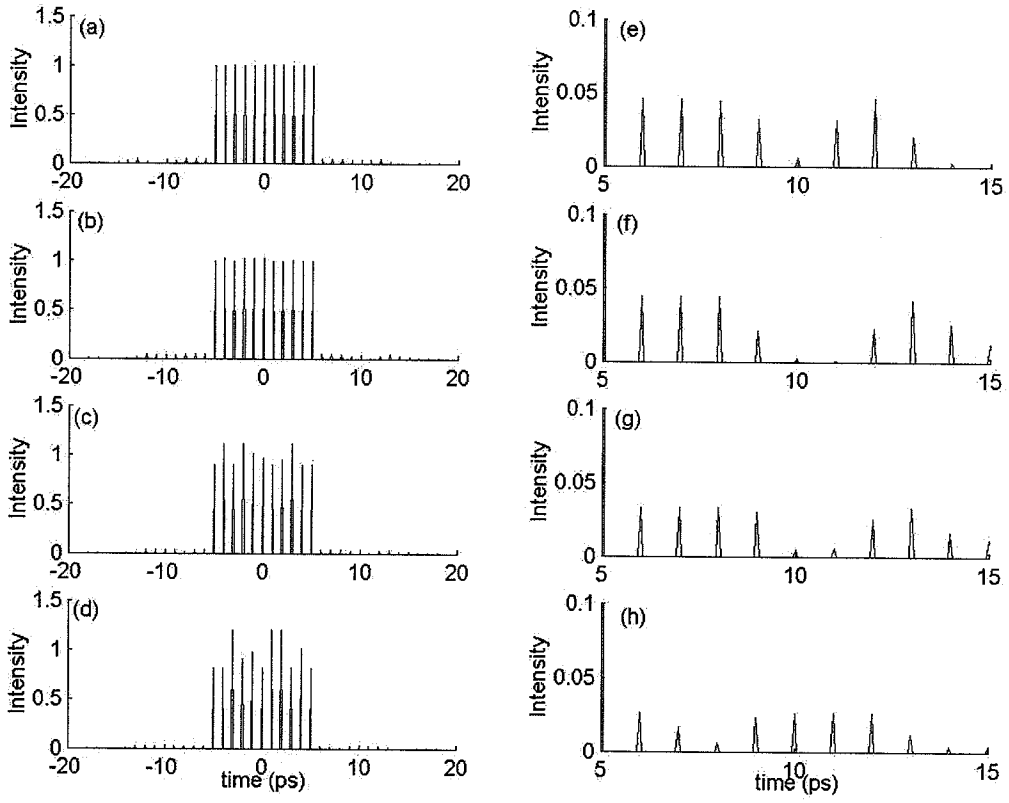


Fig. 4.8. Output temporal intensity profiles corresponding to points (a), (b), (c) and (d) on the trade-off curve, (e), (f), (g) and (h) Closer look at the wing intensity corresponding to (a), (b), (c) and (d) respectively.

Table 4.7
Table of maximum intensity deviation in square envelope and wings for different extents of pathlength jitters

| $\delta L$ | Percentage Deviation in square | Percent deviation in the wings |
|---|---|---|
| Unperturbed | 0.5% | 4.6% |
| $\pm\frac{\lambda}{50}$ | 2% | 6% |
| $\pm\frac{\lambda}{25}$ | 4% | 6% |
| $\pm\frac{\lambda}{16}$ | 10% | 5.5% |
| $\pm\frac{\lambda}{8}$ | 15% | 8.5% |
| $\pm\frac{\lambda}{4}$ | 40% | 11% |

We have simulated random phase errors using a uniformly distributed random number generator. We have used he design (a) of the trade-off curve for our analysis. We generate random numbers of the order of error we want to introduce and randomly add or subtract them with the design phases. This simulation is performed 25 times and the most degraded system is presented. Our design was found to be quite tolerant to different orders of phase error. However the system begins to break down at path length shifts of about $\pm\frac{\lambda}{4}$. Fig. 4.9 shows the various changes in the output profile and spectrum induced by these changes. Note that the temporal profile still stays within a 10 percent variation in intensity in the square region, even with path length changes in the order of a one-sixteenth of a wavelength. It is thus seen that at our system is quite tolerant to path length jitters. Table 4.7 shows the tolerance of the design for various extents of pathlength jitters. Fig 4.10 shows that the spectral profiles do not change much even with a perturbation of $\pm\frac{\lambda}{8}$. Consequently the insertion loss does not get perturbed much even in this worst case.

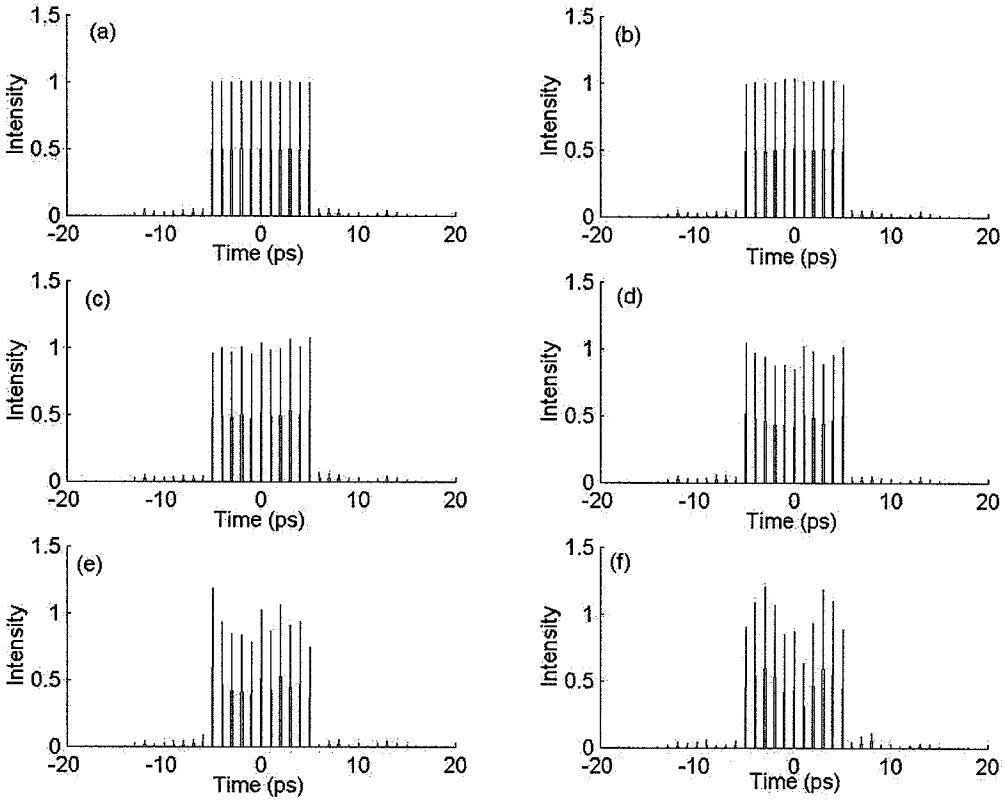


Fig. 4.9. Output temporal profiles for various pathlength jitters: (a) the unperturbed output (b) $\frac{\lambda}{100}$ (c) $\frac{\lambda}{50}$ (d) $\frac{\lambda}{32}$ (e) $\frac{\lambda}{16}$ (f) $\frac{\lambda}{8}$

## 4.5 conclusion

In this chapter, we have realized a design step by step, analyzed it for various trade-offs and finally verified the robustness of it. In general we can repeat the whole analysis for a different target number of pulses, starting off with the same procedure. We have observed that the system performs satisfactorily with respect to relative excess insertion loss. Hence these designs show good prospect to be realized experimentally.

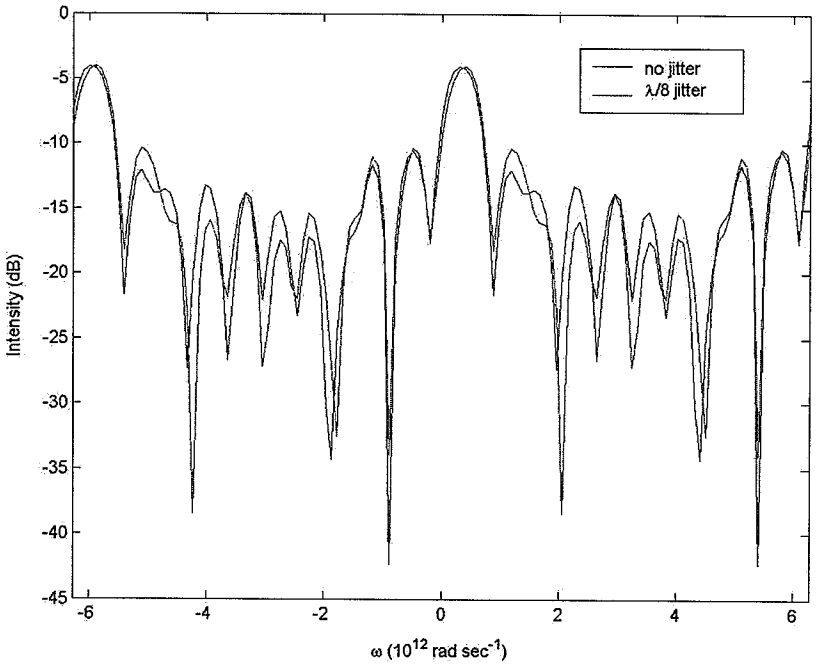


Fig. 4.10. Comparison of output spectral profiles (a) unperturbed spectrum (b) $\frac{\lambda}{8}$ jitter.

# 5. CONCLUSIONS AND FUTURE WORK

We once again state the results with aims as follows:

1. Design of a Double Passed AWG system, that employs the phase only system to femtosecond pulse sequence processing. Design for a flat topped pulse sequence.

2. Satisfactory temporal profiles, with good spectral characteristics. The square pulses corresponding to 0.2 percent variation in flatness of top, and 4 percent maximum intensity in wings, can be designed with an excess insertion loss of about 4.5 dB.

3. These designs are robust to about 5 to 8 percent variation in the flatness for pathlength jitters in the order of a sixteenth of a wavelength. Variation in the wing intensity has more or less been about 4 percent. Excess insertion loss has almost remained constant.

It would thus be very intersting to realize these designs through experiments, through fabrication of special AWGs with phase modulation. Nevertheless, with such engineered AWGs, these designs should possibly yield excellent results.

## 5.1 Future Scope

Fig. 5.1 shows an alternate realization of this situation. Here two different devices are connected back to back rather than retro reflecting from a mirror to the same device. With added degrees of freedom, this configuration offers new possibilities for better realization of the functionalities realized in our work. There could also be other novel applications that can be explored using two devices, using the systems approach and optimization technique that was used here.

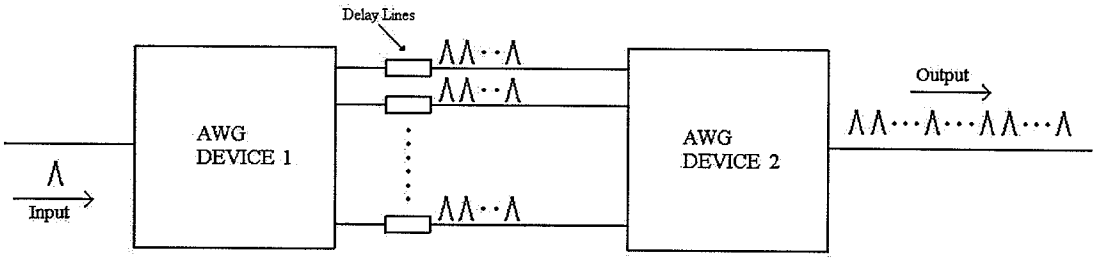


Fig. 5.1. Block Diagram of an alternate configuration using 2 AWGs.

# LIST OF REFERENCES

## LIST OF REFERENCES

[1] D. E. Leaird, S. Shen, A. M. Weiner, A. Sugita, S. Kamei, M. Ishii, and K. Okamoto. Generation of high repetition rate wdm pulse trains from an arrayed-waveguide grating. *IEEE Photonics Technology Letters*, 11(3):221–223, March 2001.

[2] D. E. Leaird, A. M. Weiner, S. Shen, A. Sugita, S. Kamei, M. Ishii, and K. Okamoto. High repetition rate femtosecond wdm pulse generation using direct space-to-time pulse shapers and arrayed waveguide gratings. *Optical and Quantum Electronics*, 33:811–826, March 2001.

[3] D. E. Leaird, S. Shen, A. M. Weiner, A. Sugita, S. Kamei, M. Ishii, and K. Okamoto. Femtosecond pulse sequence processing using a double-passed arrayed waveguide grating. *Lasers and Electro-Optics, 2002. CLEO '02. Technical Digest. Summaries of Papers*, 1:114–115, May 2002.

[4] D. E. Leaird and A. M. Weiner. Femtosecond direct space-to-time pulse shaping. *IEEE journal of Quantum Electronics*, 37(4):494–504, April 2001.

[5] D. E. Leaird, S. Shen, A. M. Weiner, A. Sugita, S. Kamei, M. Ishii, and K. Okamoto. Generation of flat-topped 500-ghz pulse bursts using loss engineered arrayed-waveguide grating. *IEEE Photonics Technology Letters*, 14(6):816–818, June 2002.

[6] A. M. Weiner. Femtosecond pulse processing. *Optical and Quantum Electronics*, 32:473–487, April 2000.

[7] A. M. Weiner. Femtosecond pulse shaping using spatial light modulators. *Review of Scientific Instruments*, 71:1929–1960, 2000.

[8] M. K. Smit. New focussing and dispersive planar component based on an optical phased array. *Electronics Letters*, 24(7):385–386, March 1988.

[9] MATLAB Optimization Toolbox. Multiobjective optimization. *Mathworks.*

[10] K. Schittkowski. Nlqpl: A fortran-subroutine solving constrained nonlinear programming problems. *Annals of Operations Research*, 5:485–500, June 1985.

[11] S. Boyd and L. Vandenberghe. *Convex Optimization.* draft of the textbook to be published, 2003.

[12] P. Munoz, D. Pastor, J. Capmany, and S. Sales. Analytical and numerical analysis of phase and amplitude errors in the performance of arrayed waveguide gratings. *IEEE journal of selected topics in Quantum Electronics*, 8(6):494–504, December 2002.

[13] M. K. Smit. Phasar-based wdm-devices: Principles, design and applications. *IEEE Journal of selected topics in Quantum Electronics*, 2(2):236–250, June 1996.

[14] H. Takahashi, K. Oda, H. Toba, and Y. Inoue. Transmission characteristics of arrayed waveguide n by n multiplexer. *IEEE Journal of Lightwave Technology*, 13(3):447–455, March 1995.

[15] K. Okamoto. Planar waveguide technology. *Digest of LEOS topical meetings*, 4:41–42, July 2000.

[16] K. Okamoto. Tutorial: Fundamentals, technology and applications of awgs. *ECOC' 98*, September 1998.